The Astronomical Journal, 153:121 (7pp), 2017 March https://doi.org/10.3847/1538-3881/aa5be2

Precession of Mercury's Perihelion from Ranging to the *MESSENGER* Spacecraft

Ryan S. Park[1], William M. Folkner[1], Alexander S. Konopliv[1], James G. Williams[1], David E. Smith[2], and Maria T. Zuber[2]
[1] Jet Propulsion Laboratory, California Institute of Technology, Pasadena, California 91109, USA; Ryan.S.Park@jpl.nasa.gov
[2] Department of Earth, Atmospheric and Planetary Sciences, Massachusetts Institute of Technology, Cambridge, Massachusetts 02139, USA
Received 2016 December 20; revised 2017 January 17; accepted 2017 January 21; published 2017 February 21

Abstract

The perihelion of Mercury's orbit precesses due to perturbations from other solar system bodies, solar quadrupole moment (J_2), and relativistic gravitational effects that are proportional to linear combinations of the parametrized post-Newtonian parameters β and γ. The orbits and masses of the solar system bodies are quite well known, and thus the uncertainty in recovering the precession rate of Mercury's perihelion is dominated by the uncertainties in the parameters J_2, β, and γ. Separating the effects due to these parameters is challenging since the secular precession rate has a linear dependence on each parameter. Here we use an analysis of radiometric range measurements to the *MESSENGER* (*MErcury Surface, Space ENvironment, GEochemistry, and Ranging*) spacecraft in orbit about Mercury to estimate the precession of Mercury's perihelion. We show that the *MESSENGER* ranging data allow us to measure not only the secular precession rate of Mercury's perihelion with substantially improved accuracy, but also the periodic perturbation in the argument of perihelion sensitive to β and γ. When combined with the γ estimate from a Shapiro delay experiment from the Cassini mission, we can decouple the effects due to β and J_2 and estimate both parameters, yielding $(\beta - 1) = (-2.7 \pm 3.9) \times 10^{-5}$ and $J_2 = (2.25 \pm 0.09) \times 10^{-7}$. We also estimate the total precession rate of Mercury's perihelion as $575.3100 \pm 0.0015''$/century and provide estimated contributions and uncertainties due to various perturbing effects.

Key words: astrometry – celestial mechanics – ephemerides – planets and satellites: individual (Mercury) – relativistic processes – Sun: interior

1. Introduction

It is well known that the longitude of perihelion of Mercury's orbit precesses along its orbit plane due to perturbations from the other solar system bodies, oblateness of the Sun, and from non-Newtonian gravitational effects (Roy 1978). The secular part of the static non-Newtonian precession was detectable before Einstein's General Theory of Relativity (GTR) was published (Le Verrier 1859; Newcomb 1882; Newcomb 1895), and later became one of the first confirmations of GTR (Einstein 1916). Our paper presents the current state of knowledge of the precession of Mercury's perihelion and associated physical parameters determined from the ranging measurements acquired by the *MESSENGER* (*MErcury Surface, Space ENvironment, GEochemistry, and Ranging*) spacecraft (Solomon et al. 2001; Smith et al. 2012).

The orbits and masses of the solar system bodies are quite well known, thus the uncertainty in the precession of Mercury's perihelion is dominated by the uncertainties in the solar oblateness, J_2, and non-Newtonian gravitational effects, which partly depend on the parameterized post-Newtonian (PPN) parameters β and γ (Will & Nordtvedt 1972). Separating the effects due to these parameters is challenging since the secular precession rate has a linear dependence on each parameter.

We show that *MESSENGER* ranging data allows us to measure not only the secular precession rate of Mercury's perihelion with substantially improved accuracy, but also the periodic perturbation in the argument of perihelion of Mercury's orbit during each orbital period that is proportional to a linear combination of β and γ. When combined with a γ estimate from the Cassini mission (Bertotti et al. 2003), i.e., $(\gamma - 1) = (2.1 \pm 2.3) \times 10^{-5}$, we can decouple the effects due to β and J_2. We also estimate the total precession rate of Mercury's perihelion and provide estimated contributions and uncertainties due to various perturbing effects, similar to a table by Clemence (1947), but with significant improvements in accuracy.

2. Dynamical Effects on Precession of Mercury's Perihelion

Of the non-Newtonian perturbations of Mercury's orbit, the perihelion motion is largest. To aid interpretation, we discuss the perihelion motion along Mercury's orbit plane from solar oblateness and non-Newtonian effects, but note that there are smaller perturbations of other elements. The rate of precession of Mercury's perihelion along its orbit plane is typically represented as $\dot{\varpi} = \dot{\omega} + \dot{\Omega}\cos i$, where i is the inclination of the orbit plane with respect to a reference plane (e.g., the solar equator or the ecliptic), $\dot{\Omega}$ is the rate of longitude of the ascending node on the reference plane, and $\dot{\omega}$ is the rate of argument of perihelion with respect to that node (Iorio 2008, 2012). Most (~92%) of this rate is due to perturbations on Mercury's orbit by the other planets, primarily Venus, Jupiter, and Earth. Considering that the orbits and masses of planets are known quite accurately, the estimate of the precession rate is limited by the uncertainties in the non-Newtonian gravitational effects and solar oblateness.

The main relativistic contribution to the secular precession of Mercury's orbit comes from the distortion of space-time by the Sun's mass (sometimes called the gravitoelectric (GE) effect). In the PPN formulation (Will & Nordtvedt 1972; Iorio 2008), the GE effect can be stated as

$$\dot{\varpi}_{\rm GE} = \frac{(2 - \beta + 2\gamma) G M_\odot n}{c^2 a (1 - e^2)}, \quad (1)$$

where β is a measure of the nonlinearity of superposition for gravity, γ is a measure of the curvature of space due to unit rest mass, G is the universal gravitational constant, $M_\odot$ is the solar mass, c is the speed of light, n is the mean motion, a is the semimajor axis, and e is the eccentricity of Mercury's orbit. The standard theory of general relativity, e.g., Einstein's GTR, assumes $\beta = \gamma = 1$. The GE effect causes a perihelion precession rate of about $43''$/century, which is about 7.5% of the total precession rate.

Another consequence of GTR is the Lense–Thirring (LT) effect (Lense & Thirring 1918), also known as the gravitomagnetic or frame-dragging effect, which is due to the additional distortion of space-time around a rotating body caused by the rotation of that body. The precession rate along the orbit plane associated with LT is given by (Iorio 2008)

$$\dot{\varpi}_{\rm LT} = -\frac{2(1+\gamma)GS_\odot \cos i}{c^2 a^3 (1-e^2)^{3/2}}, \quad (2)$$

where $S_\odot$ is the angular momentum of the Sun and i is the inclination of the solar equator to Mercury's orbit plane. We adopt the value of $S_\odot = 190 \times 10^{39}$ kg m^2 s^{-1} from helioseismology (Pijpers 1998; Mecheri et al. 2004), which gives a Mercury perihelion precession rate of about $-0.''002$/century for $\gamma = 1$ (Iorio 2005). For earlier theoretical calculation of the LT effect on the perihelion precession of Mercury based on previous estimates of Mercury's orbit and the Sun's angular momentum (see de Sitter 1916; Barker & O'Connell 1970; Cugusi & Proverbio 1978; Soffel 1989). The Earth-induced LT effect has been detected for the *LAGEOS* satellites in Earth orbit (with 10% stated uncertainty, but with ongoing evaluation; Ciufolini & Pavlis 2004; Ciufolini et al. 2011; Iorio 2011b; Renzetti 2014) and contributed to the precession of gyroscopes measured by Gravity Probe B (19%) (Everitt et al. 2011). Instead of estimating the LT effect, which is linearly proportional to $S_\odot$, we consider the effect of an uncertainty of 15×10^{39} kg m^2 s^{-1} in the estimation process (Bierman 1977), which is 10 times the reported uncertainty from helioseismology (Pijpers 1998). This constrains the value of $S_\odot$, but includes its uncertainty in the estimated solution.

The precession of Mercury's perihelion along the orbit plane due to the Sun's oblateness, i.e., quadrupole moment, J_2, is given by

$$\dot{\varpi}_{J_2} = \frac{3}{2}\frac{nJ_2}{(1-e^2)^2}\left(\frac{R_\odot}{a}\right)^2\left(1-\frac{3}{2}\sin^2 i\right), \quad (3)$$

where $R_\odot$ is the solar equatorial radius, i is the inclination between the planes of the solar equator and Mercury's orbit, and J_2 is the un-normalized solar quadrupole moment. This effect causes a perihelion precession rate of about $0.''03$/century, which is about 0.07% of the GE effect.

As shown in Equations (1)–(3), the precession rate of Mercury's perihelion has a linear dependence on the parameters β, γ, and J_2, which makes it very difficult to independently estimate these parameters by measuring the precession of the orbit of Mercury. In order to separate these parameters, two additional constraints (or observations) are required.

Although small, GTR predicts a periodic effect on the perihelion motion (Soffel 1989; Longuski et al. 2004; Park et al. 2005). In the PPN formulation, the periodic changes in Mercury's argument of perihelion can be written as

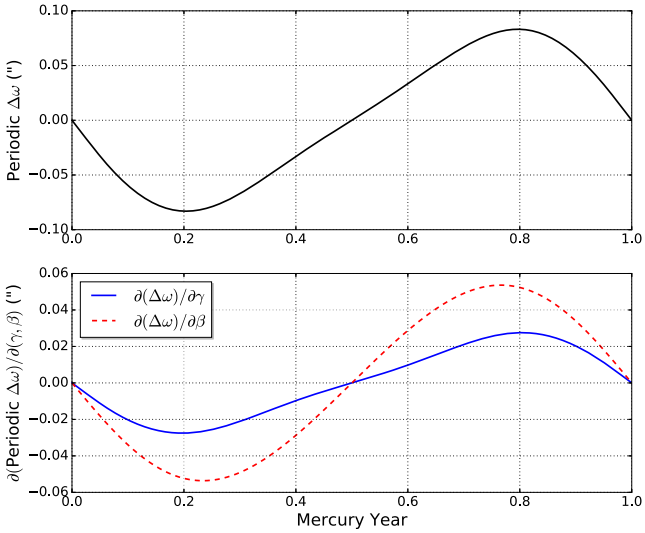

Figure 1. Periodic changes in Mercury's argument of perihelion due to the GE effect (top) and the partial derivative of $\Delta\omega$ with respect to β and γ (bottom) over one Mercury orbital period (i.e., $f = 0$–2π).

$$\Delta\omega = \frac{GM_\odot}{c^2 a(1-e^2)}\left[-\left(\frac{2\beta+(1-e^2)\gamma}{e}\right)\sin f - (2+\beta+2\gamma)\sin f\cos f\right], \quad (4)$$

where f is Mercury's true anomaly. The GE effect does not cause perturbations of the node, so precession and periodic effects on the argument and longitude of perihelion are equivalent. Figure 1 shows the periodic changes in Mercury's argument of perihelion from osculating orbital elements over one Mercury orbital period, illustrating the maximum amplitude of about $0.''08$. Considering Mercury's mean semimajor axis of 0.39 au, the maximum periodic amplitude is 22.6 km (i.e., $0.''08 \times 0.39$ au). There is a corresponding periodic effect on the radial distance from the Sun of amplitude of about $ae\Delta\omega$ or 4.6 km (using $a = 5.79 \times 10^7$ km and $e = 0.2056$). Figure 1 also shows the partial derivatives of $\Delta\omega$ with respect to β and γ, displaying maximum amplitudes of $0.''05$ ($\sim$14.1 km) and $0.''03$ ($\sim$8.5 km), respectively. The accuracy of typical spacecraft ranging is about 1 m, indicating that this periodic effect can be easily measured by accurately tracking the motion of *MESSENGER*'s orbit about Mercury.

The perturbations in the argument of perihelion of Mercury from the planets also have periodic effects, but primarily at periods different from Mercury's orbital period and the amplitudes are generally less than $10''$. The amplitudes for the planetary terms are driven by the planetary orbital elements and planetary mass parameters that are all known with accuracy better than 0.1 part per million, thus the uncertainty from these perturbations is small compared to the data noise in determining the amplitude of the GE effect. The periodic amplitude due to solar oblateness is several orders of magnitude smaller than the GE effect and is out of phase from the GE effect by about 40° in orbital longitude due to the inclined orientation of Mercury's orbit with respect to the solar angular momentum vector.

To date, the best estimate of the parameter γ comes from the Cassini solar conjunction experiment (Bertotti et al. 2003), i.e., $(\gamma - 1) = (2.1 \pm 2.3) \times 10^{-5}$. Doppler measurements of the radio signal from the spacecraft were used to determine γ from its effect on the light time between the spacecraft and the Earth from the Shapiro effect (Shapiro 1964). The Cassini measurements used radio signals at multiple frequencies to separate the Shapiro effect from the frequency-dependent delay caused by charged particles in the interplanetary media (solar plasma). The *MESSENGER* ranging data are also sensitive to the Shapiro effect and the solar plasma. Since *MESSENGER* used a single radio frequency, the effect from Shapiro delay and solar plasma cannot be separated well. Instead, we constrain the value of γ to the Cassini experiment value.

Combining the Cassini γ with measurements of both secular and periodic precession of Mercury's orbit allows estimation of both β and J_2.

3. *MESSENGER* Ranging Data and Estimated Results

Section 2 gives analytical expressions for the dynamical effects of various perturbations that affect the precession of Mercury's perihelion and current knowledge of associated parameters. This section shows how we actually estimate these fundamental parameters through a dynamical estimation process, i.e., we numerically integrate the PPN governing equations of motion with the LT effect included (Moyer 2000; Folkner et al. 2014). We also integrate the partial derivatives of the orbits of Earth and Mercury with respect to parameters that affect the dynamics, e.g., solar angular momentum $S_\odot$ and the PPN parameters β and γ. The partials of planetary coordinates are then converted to partials of the Earth–Mercury range with respect to these parameters when they are used in a least-squares solution.

Radio range and Doppler tracking measurements of the *MESSENGER* spacecraft by the NASA Deep Space Network (DSN) were acquired during the orbital science phase at Mercury (Smith et al. 2012). We first processed the Doppler data and estimated the orbit of *MESSENGER* with respect to Mercury's center of mass (COM), including a 70th degree spherical harmonic gravity field of Mercury. With the estimated orbit for *MESSENGER*, we adjusted the range measurements to Mercury's COM. Subsequently, we processed the range data, together with other observations of planetary objects (Folkner et al. 2014), to estimate the orbit of Mercury along with those of the other planets. Estimated parameters describing the orbit of Mercury include the initial position and velocity at the reference epoch for numerical integration; the solar mass parameter and solar quadrupole moment; and the PPN parameter β. The estimate list includes parameters γ and $S_\odot$, but instead of estimating them, we considered their uncertainties (Bierman 1977) with a priori uncertainties for γ from the Cassini solar conjunction experiment (i.e., 2.3×10^{-5}) and $S_\odot$ from helioseismology (i.e., 15×10^{39} kg m^2 s^{-1}). Initial conditions and parameters from the fit are used to generate a numerically integrated ephemeris of the planets.

Range measurements are typically taken every 10 minutes during DSN tracking passes (with an average duration of eight hours). Range measurement errors include a residual error in calibration of the signal path delay in the DSN tracking station performed before each tracking pass that applies to each measurement during that pass. The change in range to the spacecraft during a tracking pass is much more accurately measured by Doppler measurements, used to fit the spacecraft trajectory with respect to Mercury, than by range measurements. Therefore, there is only one independent range point from each tracking pass available for estimation of Mercury's orbit (Kuchynka & Folkner 2013). The post-fit residuals for the range measurements used in the fit are shown in Figure 2. The root-mean-square of the post-fit residuals for the range measurements used in the fit was about 0.8 m, with error contributions from the DSN signal path calibration error, error in the spacecraft orbit with respect to Mercury's COM, and effect of charged particles (solar plasma, Earth ionosphere) on the radio signal. Measurements made with the Earth–Sun–Mercury angle $>120°$ have the largest effect from solar plasma and are not included in our estimation.

Table 1 shows the recovered values of J_2 and β from processing *MESSENGER* ranging data using a least-squares estimation technique. Our estimate for the solar quadrupole moment is in good agreement with the expected value from the helioseismology value, $(2.18 \pm 0.06) \times 10^{-7}$ (Pijpers 1998). Also, compared to the current best estimate of $(\beta - 1) = (1.2 \pm 1.1) \times 10^{-4}$ from the Nordtvedt effect (Williams et al. 2004), the β uncertainty has improved by a factor of three.

We have accounted for systematic errors in the radio range calibrations as described above. To test for other systematic errors, we have estimated J_2 and β, along with orbital parameters, using two independent subsets of the *MESSENGER* range data. The first subset includes data from 2011 March through 2012 September, and the second subset from 2012 September to 2014 August. The resulting estimated values and uncertainties of J_2 and β are also given in Table 2. The results between subsets and the total are in very good agreement. We note that the estimated uncertainties do not depend strongly on the number of measurements mainly because of the considered effect of γ uncertainty.

If we consider a hypothetical case where GTR is assumed to be perfect (i.e., $\gamma = \beta = 1$ exactly) without a priori information for both the value and uncertainty of the solar quadrupole moment and solar moment of inertia, our analysis yields the recovered values of $J_2 = (2.28 \pm 0.06) \times 10^{-7}$ and $S_\odot = (196 \pm 70) \times 10^{39}$ kg m^2 s^{-1}. We note that this is a limiting case that shows the potential separability between J_2 and $S_\odot$ that might be achieved if β and γ are more accurately measured. If we simultaneously estimate all four parameters J_2, $S_\odot$, γ, and β without the constraints on $S_\odot$ and γ, then the uncertainty in these parameters becomes quite large, as expected from the discussion in Section 2.

4. Estimation and Contributions to the Precession Rate of the Perihelion

Traditionally, the Mercury perihelion precession rate has been important in discussions of GTR. Analytically, the precession rate can be computed based on the Gauss perturbation equations (Roy 1978), which depend on the osculating orbit elements (Iorio 2008, 2011a, 2012). However, we wish to extract the precession rate from the post-fit numerically integrated ephemeris. There are several different methods for fitting orbital elements to the integrated motion that give slightly different results. Here, we present a step-by-step procedure for computing the precession rate of Mercury's perihelion from a numerically integrated ephemeris of

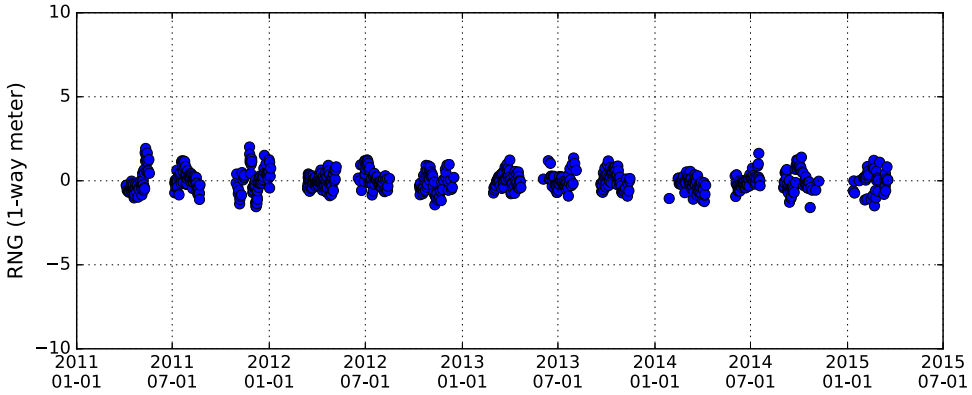

Figure 2. *MESSENGER* range measurement residuals with respect to the updated ephemeris of Mercury. The range data rms is about 0.8 one-way meter.

Table 1
Estimated Values and Uncertainties of Solar J_2 and PPN β from Processing *MESSENGER* Ranging Data

Parameter	$J_2 \times 10^7$	$(\beta - 1) \times 10^5$
Total	2.25 ± 0.09	-2.6 ± 3.9
Subset 1	2.26 ± 0.09	-2.8 ± 4.0
Subset 2	2.28 ± 0.09	-3.2 ± 4.0

Table 2
Estimated Periodic Amplitudes of Mercury's Longitude of Perihelion

Frequencies (υ_i)	S_i ($''$)	C_i ($''$)	Total Amplitudes $\sqrt{S_i^2 + C_i^2}$ ($''$)
$0n_M + 2n_V$	−0.44	−0.24	0.50
$0n_M + 1n_V$	0.19	−0.70	0.73
$1n_M - 2n_V$	−3.67	2.55	4.47
$2n_M - 3n_V$	−0.55	−0.38	0.67
$1n_M - 3n_V$	1.93	1.55	2.48
$2n_M - 4n_V$	0.25	−0.78	0.82
$2n_M - 5n_V$	3.37	0.05	3.37
$1n_M - 2n_E$	0.46	−0.61	0.76
$1n_M - 4n_E$	−0.21	−0.54	0.58
$0n_M + 3n_J$	0.42	−0.63	0.76
$0n_M + 2n_J$	0.39	−7.23	7.24
$0n_M + 1n_J$	−0.55	1.44	1.54
$1n_M - 2n_J$	0.16	0.82	0.83
$0n_M + 2n_S$	0.50	−0.71	0.86

Note. The parameters n_M, n_V, n_E, n_J, and n_S denote the mean motion of Mercury, Venus, Earth, Jupiter, and Saturn, respectively.

Mercury. This procedure is based on the mean Mercury orbital angular momentum frame defined below.

First, we define Mercury's mean orbit frame by computing the R.A. and decl. of Mercury's orbital angular momentum vector based on a 2000 year long trajectory (i.e., from 1000 January 1 to 3000 January 1). The corresponding R.A. and decl. of the mean orbit pole vector yield $\alpha_M = 280.^\circ9876$ and $\delta_M = 61.^\circ4481$ with respect to the International Celestial Reference Frame (ICRF; Ma et al. 2009). The inertial mean Mercury orbital frame can be defined with these two angles (defining the z-axis), and by assuming that the y-axis is determined by the cross product of the z-axis with ICRF x-axis; the orbit frame x-axis completes the triad. Note that the orientation of the orbit plane changes by $<60''$/century and it affects the precession rate by $<0.''0001$/century, which is below what can be measured from *MESSENGER* ranging data. The solar equator plane is inclined by $\sim 3.^\circ4$ to the mean plane of Mercury's orbit given above.

From the ephemeris, we then compute the times of Mercury's perihelion passages during this 2000 year time span, compute the position vector and project it onto the frame defined by the mean orbit pole vector, and compute the change in angle with respect to the initial position vector in the projected frame to determine the change in longitude of perihelion. Figure 3(a) shows the change in the precession angle of Mercury's perihelion during the 2000 year time span. It is important to note that the perihelion of Mercury does not change linearly with time; there are periodic perturbations from the planets superposed on the linear advance, as Figure 3(b) shows. Venus and Jupiter contribute the largest variations, followed by Earth and Saturn. The 2000 year time span used for fitting the rate should reduce the influence of the periodic terms on the average rate.

Lastly, the precession rate of Mercury's perihelion is determined by computing the slope of this angle based on fitting a quadratic plus periodic fit, i.e., $B + \dot{\varpi}t + Qt^2 + \sum_{i=1}^{N}(S_i \sin \upsilon_i t + C_i \cos \upsilon_i t)$ with the epoch of 2000 January 1. We have estimated amplitudes (S_i and C_i) of all frequencies (υ_i) that contribute $\geqslant 0.''5$ to the longitude of perihelion, which resulted in a total of 14 periods (see Table 2). The total precession rate determined from this procedure yields $\dot{\varpi} = 575.''3100$/century with the quadratic term of $Q = -0.''04478132$/century^2. Table 2 shows the estimated periodic amplitudes.

Note that the precession rate derived above by fitting the longitude of perihelion over 2000 years of integration is simply a process to reduce the numerical error of the extracted precession rate. The precession rate is primarily due to the effect of linear combinations of parameters estimated in the ephemeris fit, including the initial state of Mercury and the other planets, J_2, PPN parameters, etc., as determined from the *MESSENGER* ranges taken over a span of four years. The precession rate derived in this way is unique, within uncertainties, independent of the exact values of the constrained parameters (e.g., on γ from Cassini). The combination of parameters, regardless of constraints used, must give the same precession rate in order to fit the *MESSENGER* range data. The uncertainty in the precession rate is dominated by the estimated uncertainty in β and J_2 from fitting the *MESSENGER* data plus the uncertainty in γ from Cassini.

In Table 3, we show the breakdown of estimated contributions to the precession of perihelion of Mercury and uncertainties from the planets, asteroids, GE effect, LT effect,

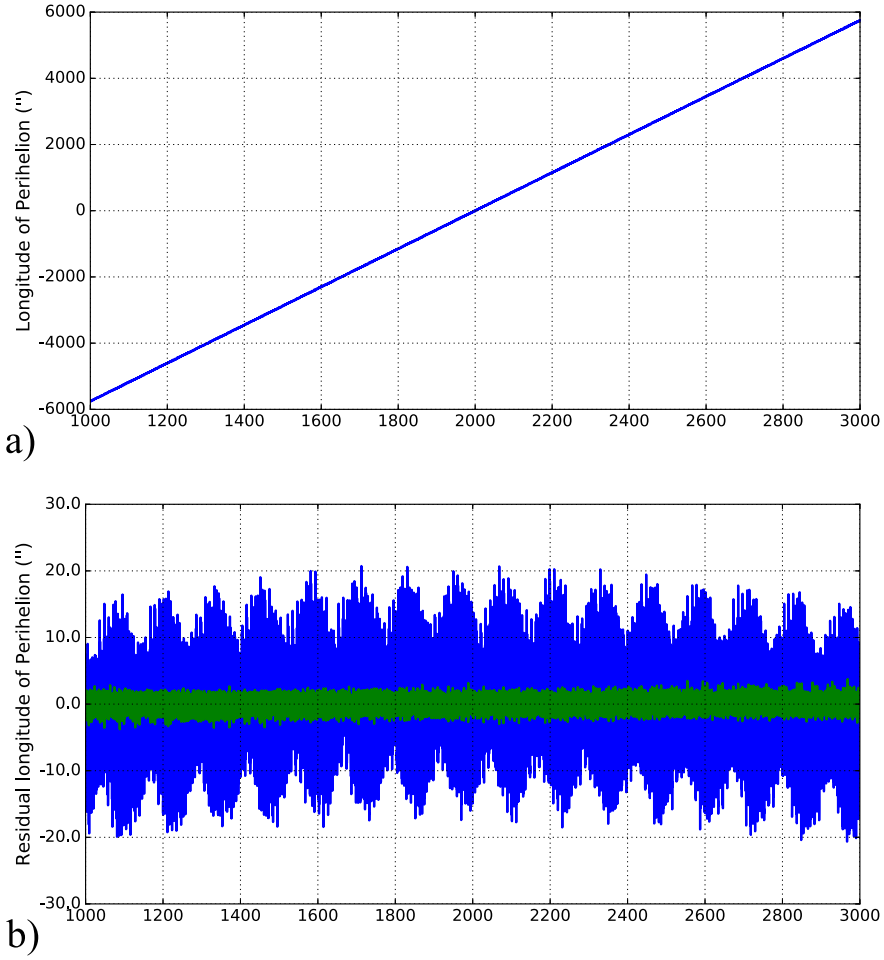

Figure 3. (a) The precession of Mercury's perihelion in the plane perpendicular to $\alpha_M = 280.^{\circ}9876$ and $\delta_M = 61.^{\circ}4481$. The rate estimate of this plot gives the precession rate of $575.''3100$/century. (b) The residual precession angle has a linear fit removed (blue) and a quadratic plus periodic fit removed (green).

and solar quadrupole moment. This is similar to a table by Clemence (1947) with significant improvements in accuracy and including additional effects. Also, the observed GE precession was estimated in Clemence by subtracting the computed planetary effects from the total measured precession of perihelion of Mercury, whereas we determine the GE effect by isolating it in the numerically integrated ephemeris as described below.

The effect of Mercury on its perihelion precession rate was computed by integrating the planetary ephemeris with the mass parameter (GM) of Mercury set to zero and evaluating the difference in the perihelion precession rate from the nominal ephemeris. The main effect due to the Mercury mass parameter comes from its effect on the orbit of Venus and the other planets. The average acceleration of Mercury on Venus is dominated by an effective quadrupole moment due to the mass of Mercury orbiting the Sun. This results in a change in the Venus mean motion and other elements, much like the solar J_2 causes, but much larger. The change in the Venus orbit then changes the effect of Venus on the Mercury perihelion precession rate. Smaller changes in the perihelion precession rate due to the Mercury mass parameter come from the change in the shape of the orbit of Mercury about the Sun and from the interaction of Mercury's J_2 and C_{22} with the Sun. The change in the precession rate due to Mercury's J_2 and C_{22} is $\sim 0.''00036$/century, which is included in the term due to Mercury in Table 3 (i.e., $0.''0050$/century). The values of Mercury's J_2 and C_{22} come from Mazarico et al. (Mazarico et al. 2014). The estimated uncertainty in the Mercury line for precession rate in Table 3 is mainly due to the uncertainty in Mercury's GM.

The effects on the Mercury perihelion precession due to the other planets have been computed in a similar manner. The effect for each planet comes from both its direct effect on Mercury and indirect effects due to the changes in the orbits of the other planets. Table 3 shows both direct and indirect effects. For example, the Venus row represents the difference in Mercury's precession rate when the mass of Venus is set to zero, thus the direct effect of Venus. The "Venus+Earth/Moon" row represents the change in precession due to the change in the Earth's orbit when the GM of Venus is set to zero, thus noted as the indirect effect.

The uncertainties in the effects of the planets on the precession rate shown in Table 3 include the estimated uncertainties in their orbits from this analysis and the uncertainties in their mass parameters. The mass parameters and uncertainties of the planets were taken from a separate analysis of radio tracking data of orbiting spacecraft (Konopliv et al. 1999, 2011; Jacobson et al. 2000, 2006). The mass parameters of Earth and Moon were derived from planetary and lunar laser ranging (Folkner et al. 2014), which are compatible with results from satellite laser ranging of *LAGEOS*

Table 3
The Breakdown of Estimated Contributions and Uncertainties from the Planets, Asteroids, GE effect, LT effect, and Solar Quadrupole Moment to the Precession Rate of Mercury's Perihelion Computed in the coordinate Frame Defined in Section 4 (i.e., along Mercury's Mean Orbit Plane)

Effects	Precession Rate of Perihelion, $\dot{\varpi}$ ($''$/Julian century)
Mercury	$0.0050 \pm <0.0001$
Mercury+Venus Interaction	-0.0053
Venus	$277.4176 \pm <0.0001$
Venus+Earth/Moon Interaction	-0.0209
Venus+Jupiter Interaction	-0.0012
Earth/Moon	$90.8881 \pm <0.0001$
Earth/Moon+Mars Interaction	-0.0016
Mars	$2.4814 \pm <0.0001$
Mars+Jupiter Interaction	0.0002
Jupiter	$153.9899 \pm <0.0001$
Jupiter+Saturn Interaction	0.0411
Saturn	$7.3227 \pm <0.0001$
Saturn+Uranus Interaction	0.0004
Uranus	$0.1425 \pm <0.0001$
Neptune	$0.0424 \pm <0.0001$
Asteroids	$0.0012 \pm <0.0001$
Solar Oblateness	0.0286 ± 0.0011
Gravitoelectric (Schwarzschild-like)	42.9799 ± 0.0009
Lense–Thirring (Gravitomagnetic)	-0.0020 ± 0.0002
Total	575.3100 ± 0.0015

Note. This table is similar to a table by Clemence (1947) with significant improvements in accuracy and including additional effects.

(Ries et al. 1992) and radio tracking of the *GRAIL* spacecraft (Konopliv et al. 2013; Lemoine et al. 2013; Williams et al. 2014).

The uncertainty of the effects of the asteroids comes from the estimated mass parameters of the 343 asteroids that most perturb the orbits of the planets as included in this estimation, as described in Kuchynka & Folkner (2013). These asteroids comprise 90% of the mass of the main belt asteroids, with total uncertainty large enough to encompass the unmodeled asteroids.

The perihelion precession due to LT was computed by comparing the nominal ephemeris with an integration performed with the solar angular momentum set to zero, with uncertainty determined from the uncertainty in the solar angular momentum. The precession rate due to solar oblateness is computed in the same manner (i.e., J_2 set to zero) and the uncertainty in its effect comes from the estimated uncertainty of J_2 given in Table 1. The precession due to the GE effect was computed by comparing the precession from the integration with the speed of light essentially infinite, then subtracting the effect due to LT and planetary GM contributions in the PPN formulation. Note that this procedure is essentially equivalent to the difference between the nominal ephemeris with an ephemeris integrated with all of the GM values (except for the Sun), J_2 and $S_\odot$ set to zero and the speed of light set to infinity. The uncertainty in the GE contribution was determined by the uncertainty in γ from the Cassini determination (Bertotti et al. 2003) and β from *MESSENGER* ranging.

The uncertainty in the total precession rate (i.e., $0\farcs0015$/century) is simply the root-sum-square of the uncertainties shown in Table 3. Note that the uncertainty in the precession rate is smaller than the LT effect, thus the LT effect must be modeled to achieve this level of accuracy, and thus the LT effect is consistent at ~75% accuracy.

5. Conclusions

We have processed the *MESSENGER* ranging data as a part of JPL's planetary ephemeris development process. Constraining the PPN parameter γ from the Cassini solar conjunction experiment and the Sun's angular momentum from helioseismology, we show that *MESSENGER* ranging data allow us to separate the effects due to the PPN parameter β and the solar oblateness J_2. The resulting estimates give $(\beta - 1) = (-2.7 \pm 3.9) \times 10^{-5}$ and $J_2 = (2.25 \pm 0.09) \times 10^{-7}$. We also estimate the total precession rate of Mercury's perihelion of $(575.3100 \pm 0.0015)''$/century that corresponds to our solution and provide estimated contributions and uncertainties due to various perturbing effects.

We thank the *MESSENGER* project for providing information regarding spacecraft activities. This research was carried out in part at the Jet Propulsion Laboratory, California Institute of Technology, under contract with the National Aeronautics and Space Administration. J.G.W. discussed secular and periodic relativistic terms for Mercury with J. Bootello. M.T.Z. and D.E.S. were supported by the NASA/*MESSENGER* mission, performed under contract from NASA to the Carnegie Institution of Washington and Columbia University.

References

Barker, B. M., & O'Connell, R. F. 1970, PhRvD, 2, 1428
Bertotti, B., Iess, L., & Tortora, P. 2003, Natur, 425, 374
Bierman, G. 1977, Factorization Methods for Discrete Sequential Estimation (New York: Academic)
Ciufolini, I., & Pavlis, E. C. 2004, Natur, 431, 958
Ciufolini, I., Paolozzi, A., Pavlis, E. C., et al. 2011, EPJP, 126, 72
Clemence, G. M. 1947, RvMP, 19, 361
Cugusi, L., & Proverbio, E. 1978, A&A, 69, 321
de Sitter, W. 1916, MNRAS, 76, 699
Einstein, A. 1916, AnP, 49, 769
Everitt, C. W. F., DeBra, D. B., Parkinson, B. W., et al. 2011, PhRvL, 106, 221101
Folkner, W. M., Williams, J. G., Boggs, D. H., Park, R. S., & Kuchynka, P. 2014, The Planetary and Lunar Ephemeris DE 430 and DE 431, The Interplanetary Network Progress Rep. 42-196 (Pasadena, CA: Jet Propulsion Laboratory)
Iorio, L. 2005, A&A, 431, 385
Iorio, L. 2008, ScReE, 2008, 105235
Iorio, L. 2011a, IJMPD, 20, 181
Iorio, L. 2012, SoPh, 281, 815
Iorio, L., et al. 2011, Ap&SS, 331, 351
Iorio, L., Lichtenegger, H. I. M., Ruggiero, M. L., & Corda, C. 2011b, Ap&SS, 331, 351
Jacobson, R. A., Antreasian, P. G., Bordi, J. J., et al. 2006, AJ, 132, 2520
Jacobson, R. A., Haw, R. J., McElrath, T. P., et al. 2000, JAnSc, 48, 495
Konopliv, A. S., Asmar, S. W., Folkner, W. M., et al. 2011, Icar, 211, 401
Konopliv, A. S., Banerdt, W. B., & Sjogren, W. L. 1999, Icar, 139, 3
Konopliv, A. S., Park, R. S., Yuan, D.-N., et al. 2013, JGRE, 118, 1415
Kuchynka, P., & Folkner, W. M. 2013, Icar, 222, 243
Lemoine, F. G., Goossens, S., Sabaka, T. J., et al. 2013, JGRE, 118, 1676
Lense, J., & Thirring, H. 1918, PhyZ, 19, 156
Le Verrier, U. J. 1859, Theorie du mouvement de Mercure. Annales de l'Observatoir Impirial de Paris 5, 1
Longuski, J. M., Fischbach, E., Scheeres, D. J., et al. 2004, PhRvD, 69, 042001
Ma, C., Arias, E. F., Bianco, G., et al. 2009, IERS Technical Note No. 35
Mazarico, E., Genova, A., Goossens, S., et al. 2014, JGRE, 119, 2417
Mecheri, R., Abdelatif, T., Irbah, A., et al. 2004, SoPh, 222, 191
Moyer, T. D. 2000, Formulation for Observed and Computed Values of Deep Space Network Data Types for Navigation, Deep Space Communications and Navigation Series, JPL Publication 00-7. http://descanso.jpl.nasa.gov/monograph/series2/Descanso2_all.pdf

Newcomb, S. 1882, in Astronomical Papers of the American Ephemeris and Nautical Almanac, Vol. 1, Discussions and results of observations on transits of Mercury from 1677 to 1881 (Washington, DC: U.S. Nautical Almanac Office), 363
Newcomb, S. 1895, The elements of the four inner planets and the fundamental constants of Astronomy, Supplement to the American Ephemeris and Nautical Almanac (Washington, DC: U.S. Nautical Almanac Office)
Park, R. S., Scheeres, D. J., Giampieri, G., et al. 2005, JSpRo, 42, 559
Pijpers, F. P. 1998, in Helioseismic Determination of the Solar Gravitational Quadrupole Moment, Structure and Dynamics of the Interior of the Sun and Sun-like Stars 418, ed. S. Korzennik, L76
Renzetti, G. 2014, NewA, 29, 25
Ries, J. C., Eanes, R. J., Shum, C. K., et al. 1992, GeoRL, 19, 529
Roy, A. 1978, Orbital Motion (Adam Hilger Limited)
Shapiro, I. I. 1964, PhRvL, 13, 789
Smith, D. E., Zuber, M. T., Phillips, R. J., et al. 2012, Sci, 336, 214
Soffel, M. H. 1989, Relativity in Astrometry, Celestial Mechanics and Geodesy (Heidelberg: Springer)
Solomon, S. C., McNutt, R. L., Jr., Gold, R. E., et al. 2001, P&SS, 49, 1445
Will, C. M., & Nordtvedt, K., Jr. 1972, ApJ, 177, 757
Williams, J. G., Konopliv, A. S., Boggs, D. H., et al. 2014, JGRE, 119, 1546
Williams, J. G., Turyshev, S. G., Boggs, D. H., et al. 2004, PhRvL, 93, 261101